IEEE Access
Multidisciplinary | Rapid Review | Open Access Journal

Received September 13, 2020, accepted September 16, 2020, date of publication September 18, 2020,
date of current version September 30, 2020.

Digital Object Identifier 10.1109/ACCESS.2020.3024982

Multi-Band and High Gain Antenna Using AMC Ground Characterized With Four Zero-Phases of Reflection Coefficient

YAJIE GONG[1], SHUHUI YANG[1], (Member, IEEE), BIN LI[1], YINCHAO CHEN[2], (Senior Member, IEEE), FANGLU TONG[1], AND CHENYIN YU[1]

[1]Department of Communication Engineering, Communication University of China, Beijing 100024, China
[2]Department of Electrical Engineering, University of South Carolina, Columbia, SC 29208, USA

Corresponding author: Shuhui Yang (yangshuhui2016@sina.com)

ABSTRACT In this paper, a multi-band AMC-backed antenna system characterized with high gain and low-profile is proposed. It is constructed by placing a quad-band coplanar-waveguide (CPW) antenna over an AMC with four zero-phases in the reflection coefficient. The CPW antenna consists of an ornamental-pillar-shaped patch with the specially designed parasitic elements, and a defected ground structure (DGS), for the application in the frequency bands of 2.45, 3.5, 4.6 and 5.8 GHz. To improve the CPW antenna's radiation performance, an artificial magnetic conductor (AMC) ground with four zero-phases of the reflection coefficient is designed and employed as the reflector. The AMC unit cell is composed of four metallic nested rings (FMNR), whose innermost ring is connected in series to four lumped capacitors. It is observed that the proposed quad-band AMC ground can not only increase the gains of the multi-band antenna greatly but also combine the two intermediate frequency bands of the antenna into a broadband one. The prototypes of the antenna and the AMC array with 5×5 unit cells were fabricated and measured. It is found that in comparison to the antenna without AMC, the AMC-backed antenna obtains a gain enhancement by amounts of 4.93, 5.92, 5.54 and 4.95 dB at the frequencies of 2.45, 3.5, 4.6 and 5.8 GHz. The 10-dB impedance bandwidths of the AMC-backed antenna include three bands of 2.13–2.87, 3.22–4.75, and 5.54–5.86 GHz, with the corresponding relative bandwidths of 14.8%, 38.4%, and 5.3%. The proposed antenna can be potentially applied to the applications in WLAN, WiMAX, and 5G mobile communication systems.

INDEX TERMS Multi-band antenna, quad-band artificial magnetic conductor (AMC), coplanar-waveguide (CPW), gain enhancement.

I. INTRODUCTION

With the rapid development of various wireless communication systems, design of multi-band microstrip antennas has received great attention from researchers in both academic and industrial fields. Various approaches for designing multi-band antennas have been developed and investigated [1]–[4]. For example, a typical technique is to make slots on the radiation patch of microstrip antenna. As discussed in [1], by etching two mental-insulator-mental (MIM) rings on a square patch, the surface current distributions have been changed, which effectively improves radiation and leads to form a multi-band antenna. Other commonly used methods for realizing multi-band antennas include adding coupling parasitic units [2], inserting stub-resonant elements [3], as well as adopting the fractal iteration technology [4].

In practice, a single antenna structure is often inadequate to meet the high demands for multi-band communication. Thus, further efforts are required to design high standard multi-band antennas in terms of dimension, directionality, gain, and impedance bandwidth. To improve antenna gain performance, three kinds of structures are frequently used for a radiation reflector, namely, perfect electric conductor (PEC) [5], [6], partially reflecting surface (PRS) [7]–[10], and artificial magnetic conductor (AMC) [11]–[29]. As a specific type of metamaterials [30], apparently differing from other two structures, the AMC has the excellent property of

The associate editor coordinating the review of this manuscript and approving it for publication was Giovanni Angiulli.

in-phase reflection. This means it can be utilized to reflect an incident electromagnetic wave with little phase reversal, just like a perfect magnetic conductor (PMC). Hence, to achieve a gain enhancement for such an antenna, only a small distance is required between the antenna and its reflector [21], [24]. Recently, AMCs have been widely employed to enhance the gains of microstrip antennas [11]–[15].

It is worth pointing out that, most of the previous reported works are limited in using single or dual-band AMCs to improve the performances of corresponding single or dual-band antennas [11]–[25]. As shown in [17], a double layer AMC reflector was proposed, which improved the radiation performance for a loaded dipole antenna at a single frequency band. In [22], a dual-band and dual-polarized antenna backed with an AMC reflector was introduced, where the AMC has two zero-phases in the reflection coefficient and performed well in gain enhancement. Due to the difficulty in design of an AMC with three or more zero-phases in its reflection coefficient, it is a great challenge to realize a tri-band AMC-backed antenna. Until now, only a few tri-band AMC-based antennas have been reported [26]–[29]. In [27], a tri-band AMC was designed and it provided a gain enhancement for the antenna by about 267% at 2.4 GHz, but the profile of this antenna was relatively high.

To design a multi-band AMC-based antenna by getting over those mentioned limitations, in this paper, firstly, a novel quad-band antenna is designed. The design originates from a basic coplanar-waveguide (CPW) antenna with a cross-shaped radiation patch, and it is developed mainly by using the specially designed parasitic elements and the defected ground structure (DGS) technology. Then, an AMC with four metallic nested-rings (FMNR) is proposed, which has four zero-phases of the reflection coefficient. In addition, to improve the reflection performance in the highest frequency band of the AMC, four lumped capacitors are connected in series to the innermost ring of the AMC unit cell. The antenna system is constructed by placing the quad-band antenna over the FMNR-AMC plane with 5 × 5 periodic unit cells. The prototypes of the proposed FMNR-AMC and antenna were fabricated and measured. The measured results show that the 10-dB impedance bandwidths of the AMC-backed antenna achieve three bands of 2.13–2.87, 3.22–4.75, and 5.54–5.86 GHz. In comparison to the antenna without using the AMC reflector, the AMC-backed antenna obtains the gain enhancements by 4.93, 5.92, 5.54 and 4.95 dB at 2.45, 3.5, 4.6 and 5.8 GHz, respectively.

II. DESIGN PRINCIPLES

A. EVOLUTIVE DESIGN OF THE CPW ANTENNA

The top view of the proposed CPW quad-band antenna for the frequency bands centered at 2.45, 3.5, 4.6, and 5.8 GHz, is displayed in Fig. 1, whose dimension parameters are summarized in Table 1.

This antenna is constructed with a single-layer 0.035 mm-thick copper printed on an FR4 substrate with the relative permittivity of 4.4, the loss tangent of 0.02, and the thickness of 1.6 mm. It mainly consists of an ornamental-pillar-shaped patch with the specially designed parasitic elements, and a defected ground structure etched with two square rings. The antenna area is 37.26 × 28.17 mm^2. The feed line of the antenna is a CPW. The initial dimensions for a rectangular antenna were calculated through the following relations [31]:

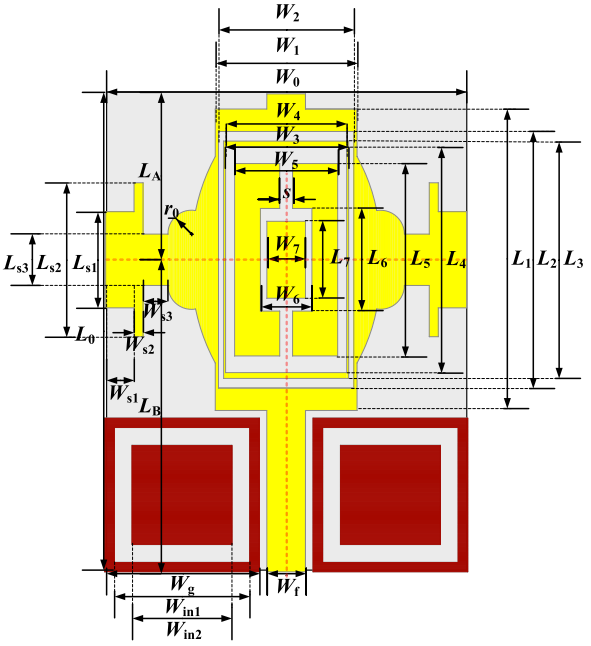

FIGURE 1. Top view of the proposed quad-band antenna.

TABLE 1. Dimension parameters for the CPW antenna.

Parameters	Value(mm)	Parameters	Value(mm)
L_0	28.17	L_A	12.93
W_0	37.26	L_B	24.33
W_1	11	L_1	23.5
W_2	10.5	L_2	20
W_3	9.7	L_3	18.5
W_4	9.4	L_4	17.6
W_5	8	L_5	15
W_6	4	L_6	8
W_7	3	L_7	6
W_{s1}	2.2	L_{s1}	7.5
W_{s2}	0.7	L_{s2}	12
W_{s3}	1.93	L_{s3}	4
W_f	3	W_g	12
W_{in1}	10.5	W_{in2}	7.75
s	1	r_0	1.86

$$w = \frac{c}{2f}\left(\frac{\varepsilon_r + 1}{2}\right)^{-\frac{1}{2}} \tag{1}$$

$$l = \frac{c}{2f\sqrt{\varepsilon_e + 1}} - 2\Delta l \tag{2}$$

$$\varepsilon_e = \frac{\varepsilon_r + 1}{2} - \frac{\varepsilon_r - 1}{2}\left(1 + \frac{12h}{w}\right)^{-\frac{1}{2}} \tag{3}$$

$$\Delta l = 0.412h\frac{(\varepsilon_e + 0.3)\left(\frac{w}{h} + 0.264\right)}{(\varepsilon_e + 0.258)\left(\frac{w}{h} + 0.8\right)} \tag{4}$$

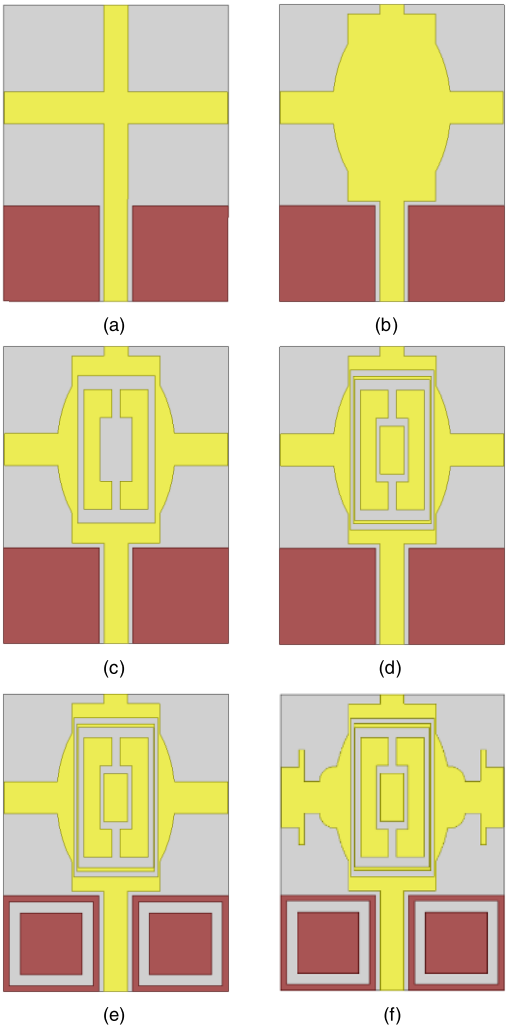

FIGURE 2. Evolution of the antenna: (a) Antenna I, (b) Antenna II, (c) Antenna III, (d) Antenna IV, (e) Antenna V, and (f) Antenna VI.

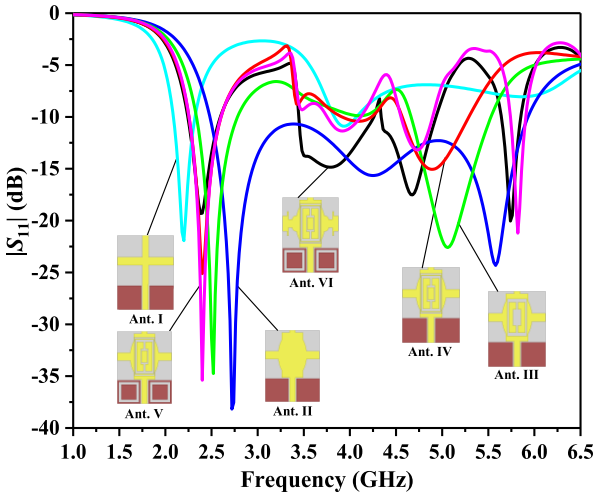

FIGURE 3. $|S_{11}|$ for six evolutive antennas.

where, l, w, Δl denote the length, width, and extension of the length of the rectangular antenna, respectively. As seen in Fig. 1, W_0 equals to w and L_0 is the sum of l and Δl. Also, h, ε_r, and ε_e listed above are, respectively, the substrate thickness, relative permittivity, and effective permittivity. In addition, c is the speed of light in free space, and f is the resonant frequency.

Using the above equations, the conventional rectangular microstrip antenna working at 2.45 GHz has the dimension of 37.26×28.17 mm^2. The evolution of the proposed antenna is illustrated in detail in Fig. 2, where six antennas are named as Antennas I to VI. The return losses ($|S_{11}|$) of the six antennas are simulated by using ANSYS HFSS and displayed in Fig. 3.

(1) As shown in Fig. 2(a), Antenna I is changed directly from a commonly used CPW rectangular antenna with a pair of square ground planes by segmenting its rectangular-shaped patch into a cross-shaped one working at a single band around 2.2 GHz (see Fig. 3).

(2) Then, a mixed elliptic and rectangular area is added to the central cross-shaped patch to form Antenna II (see Fig. 2(b)), whose operation frequency band covers from 2.53 to 5.57 GHz.

(3) Thirdly, a rectangular-ring-shaped slot is etched on Antenna II as depicted in Fig. 2(c) to change the antenna's surface current distribution and improve its resonant frequencies. In this way, Antenna III becomes a dual-band antenna resonating at 2.5 and 5.1 GHz, as shown in Fig. 3.

(4) Next, Antenna IV is constructed by reshaping its earlier version with adding a thin rectangular ring and a passive rectangular patch to the radiation patch as displayed in Fig. 2(d).

(5) Consequently, the lowest frequency band of Antenna IV successfully shifts to 2.45 GHz (see Fig. 3). After a pair of square ring grooves are etched on the ground planes of the Antenna IV to form a DGS, the Antenna V is produced as shown in Fig. 2(e), which operates at 2.45, 4.75 and 5.8 GHz, simultaneously.

(6) Finally, by inserting rectangular and circular shaped stubs into Antenna V, the final antenna, or Antenna VI (see Fig. 2(f)) is created, which generates four frequency bands around 2.45, 3.5, 4.6, and 5.8 GHz as illustrated in Fig. 3.

To further understand the working mechanism of the evolution of the proposed quad-band antenna, Fig. 4 displays the surface current distributions for Antennas I to VI.

(i) As illustrated in Fig. 4(a), Antenna I only contains the frequency band of 2.2 GHz, whose surface current at 2.2 GHz concentrates in the middle of the feed-line and parts of the ground plane.

(ii) For Antenna II, the currents distributed on the additional rectangular and elliptic area help to broaden its frequency band. As shown in Fig. 4(b), the surface currents mainly distribute along one side of the elliptic area at 5.5 GHz.

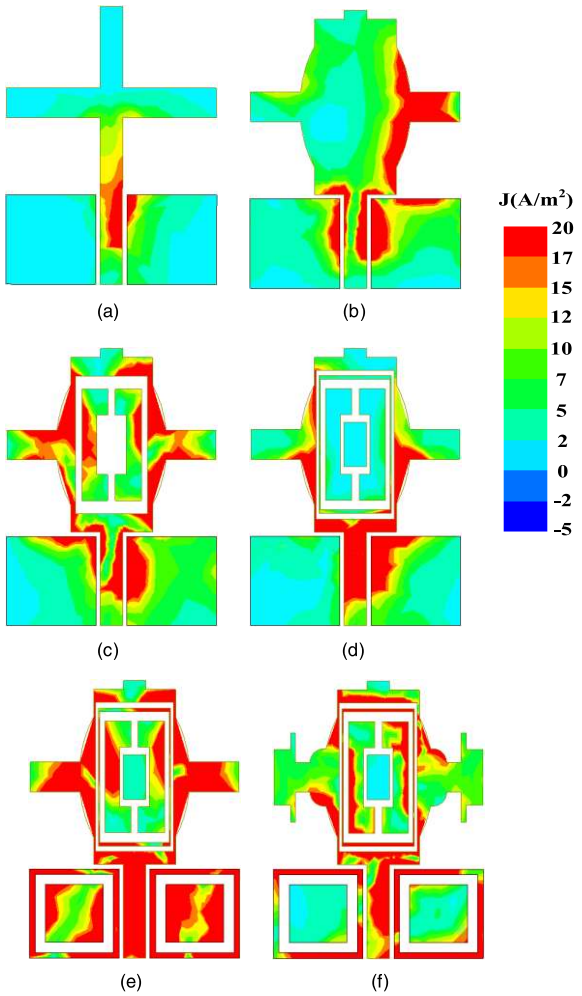

FIGURE 4. Surface current distributions for the evolution of antennas: (a) Antenna I at 2.2 GHz, (b) Antenna II at 5.5 GHz, (c) Antenna III at 5 GHz, (d) Antenna IV at 2.45 GHz, (e) Antenna V at 5.8 GHz, and (f) Antenna VI at 3.5 GHz.

(iii) After employing the dual-slit rectangular ring in Antenna III, it is obviously seen that at 5 GHz, the currents flow around both sides of the rectangle and elliptic area, even permeate into the dual-slit rectangular ring (see Fig. 4(c)). This indicates that the antenna resonant effective length is increased and more resonances move towards lower frequency bands.

(iv) Antenna III is continued to evolve into Antenna IV so that the high current density has been extend to the outskirts of the elliptic area and the short arm of the cross at 2.45 GHz as depicted in Fig. 4(d). It is noticed that for Antennas I to IV, there are no too much currents distributed on the ground plane. Thus, two square-shaped slots are etched on the ground plane in order to adjust its current distributions.

(v) As expected, the DGS of Antenna V has benefited to the antenna resonance. Meanwhile, the mixed rectangle-elliptic shaped patch also has enhanced the surface currents or the resonant effect as illustrated in Fig. 4(e).

(vi) Finally, the current distribution for Antenna VI at 3.5 GHz is displayed in Fig. 4(f). The current flowing into the added rectangular stubs is reduced, which helps to generate a new resonant frequency to make Antenna VI with four frequency bands.

The simulated S-parameters for the different values of W_{in1} and L_1 are displayed in Figs. 5 and 6. Fig. 5 illustrates that the value of W_{in1} has great impact on the return loss in the middle two frequency bands around 3.5 and 4.6 GHz, while there is almost no influence on that centered at 2.45 GHz. As W_{in1} increases, the resonant frequency of 5.8 GHz will slowly shift to the lower band. The reflection coefficients at 3.5 and 4.6 GHz are also sensitive to the alteration of L_1 as shown in Fig. 6. Differing from W_{in1}, changing L_1 not only effectively affects the return loss characteristic for 5.8 GHz band but also influences that of 2.45 GHz.

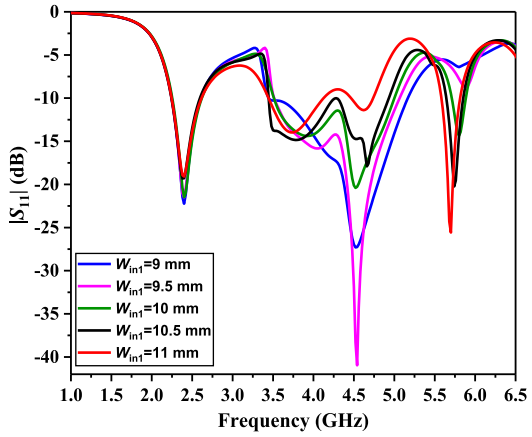

FIGURE 5. $|S_{11}|$ for different W_{in1}.

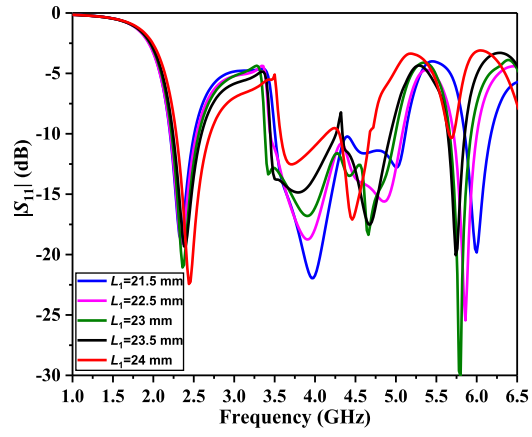

FIGURE 6. $|S_{11}|$ for different L_1.

B. DESIGN OF THE QUAD-BAND AMC

Recently, the single-band AMC has been employed as a reflector to enhance antenna gains [11]–[15]. To improve the radiation performance of the proposed quad-band CPW antenna, a new quad-band AMC structure is designed in this research, which is mainly constructed by four metallic nested rings.

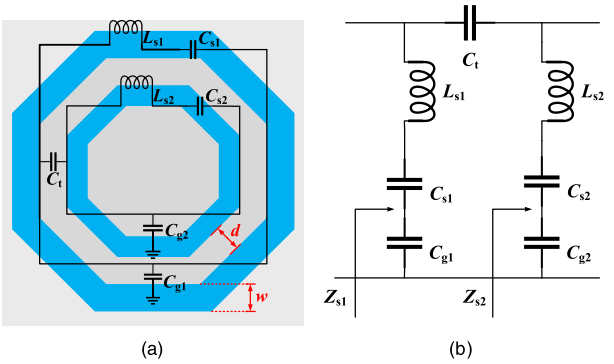

FIGURE 7. (a) Top view of the double-ring AMC structure, and (b) the equivalent circuit.

A basic double-ring AMC structure with two zero-phases of the reflection coefficient is designed as shown in Fig. 7(a). Its corresponding equivalent circuit is illustrated in Fig. 7(b). The total surface impedance of the double-ring AMC is derived as follows [25]:

$$Z_{s1} = \left[j\omega(C_{s1}//C_{g1}) + \frac{1}{j\omega L_{s1}} \right] \tag{5}$$

$$Z_{s2} = \left[j\omega(C_{s2}//C_{g2}//C_t) + \frac{1}{j\omega L_{s2}} \right] \tag{6}$$

where, Z_{s1} and Z_{s2} are the equivalent impedances of the two metal rings. L_{s1}, C_{s1}, L_{s2}, C_{s2}, C_{g1} and C_{g2} represent the patch inductance, self-capacitance and grounded capacitance introduced by the outer and inner rings. C_t denotes the gap mutual capacitance between two rings, and ω is the resonant angular frequency. When Z_{s1} and Z_{s2} are enforced to be infinite, the denominators of (7) and (8) become zero, and then the two resonant frequencies are determined as

$$f_1 = \frac{1}{2\pi\sqrt{\frac{L_{s1}C_{s1}C_{g1}}{C_{s1}+C_{g1}}}} \tag{7}$$

$$f_2 = \frac{1}{2\pi\sqrt{\frac{L_{s2}C_{s2}C_{g2}C_t}{C_{s2}C_{g2}+C_{s2}C_t+C_{g2}C_t}}} \tag{8}$$

From equations (5), (6), (7), and (8), it is seen that the total surface impedance of the double-ring AMC and its resonant frequencies are highly dependent on the equivalent distribution components (see Fig. 7(b)).

The equations for estimating these distribution components in Fig. 7(b) can be given as the following [34], [35]:

$$L_s = \mu_0 \frac{h_2 \cdot l_{effr}}{w} \tag{9}$$

$$C_s = \varepsilon_0 \varepsilon_r \frac{S_r}{t_c} \tag{10}$$

$$C_g = \varepsilon_0 \varepsilon_r \frac{S_r}{h_2} \tag{11}$$

$$C_t = \varepsilon_0 \frac{t_c \cdot l_{effr}}{d} \tag{12}$$

where, μ_0 and ε_0 are the permeability and permittivity of free space, ε_r is the relative dielectric permittivity of the substrate, h_2 is the thickness of the AMC's substrate, and S_r, l_{effr}, and t_c denote the area, efficient length and thickness of the metal ring. d and w represent the distance between the two metal rings and the width of the rings, respectively. The values of the lumped components in Fig. 8(b) are calculated and summarized as follows: L_{s1} = 15.77 nH, L_{s2} = 11.45 nH, C_{s1} = 0.14 pF, C_{s2} = 8.8 pF, C_{g1} = 2.51 pF, C_{g2} = 2.51 pF, and C_t = 0.1 pF. The phase distribution of the reflection coefficient for the dual-band AMC calculated from the equivalent circuit is simulated by using ANSYS Designer and is plotted in Fig. 8. As a comparison, the simulation result with HFSS is also shown in Fig. i8.

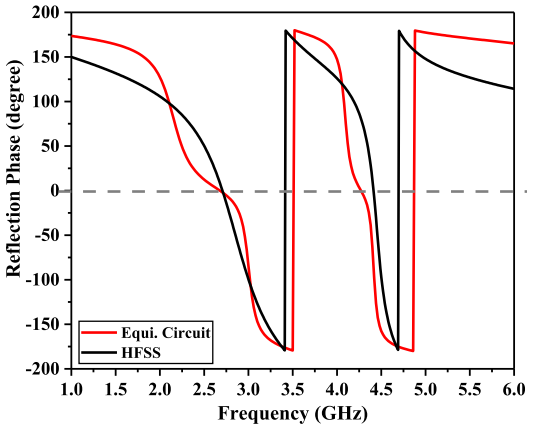

FIGURE 8. The phase distribution of the reflection coefficients for the dual-band AMC calculated from the equivalent circuit and HFSS.

As displayed in Fig. 8, the phase distribution of the reflection coefficient calculated from the equivalent circuit model is essentially consistent with the result simulated by using HFSS. This principally verifies the equivalent circuit for the double-ring AMC structure.

Fig. 9 shows the phases of the reflection coefficients with the different values of d and w. The value of d primarily impacts on the high frequency band for the AMC. The two zero-phases of the reflection coefficient both are sensitive to the width of the rings. With the increase of w, the two resonant frequencies of the double-ring AMC shift to the higher frequency bands, simultaneously.

Based on the analysis for the above double-band AMC with two metallic rings, a quad-band AMC is proposed, which originates from the single square ring AMC. The evolution process from AMC I to AMC V is illustrated in Fig. 10 and the corresponding reflection phases are plotted in Fig. 11. The physical parameters for AMC V are listed in Table 2.

When there is only one square metal ring in AMC I, one zero-phase of the reflection coefficient occurs at 2.45 GHz. Then, AMC II is formed by adding a smaller octagonal ring to AMC I, its reflection coefficient shows two zero-phases at 2.45 and 3.5 GHz. Similarly, through utilizing three and

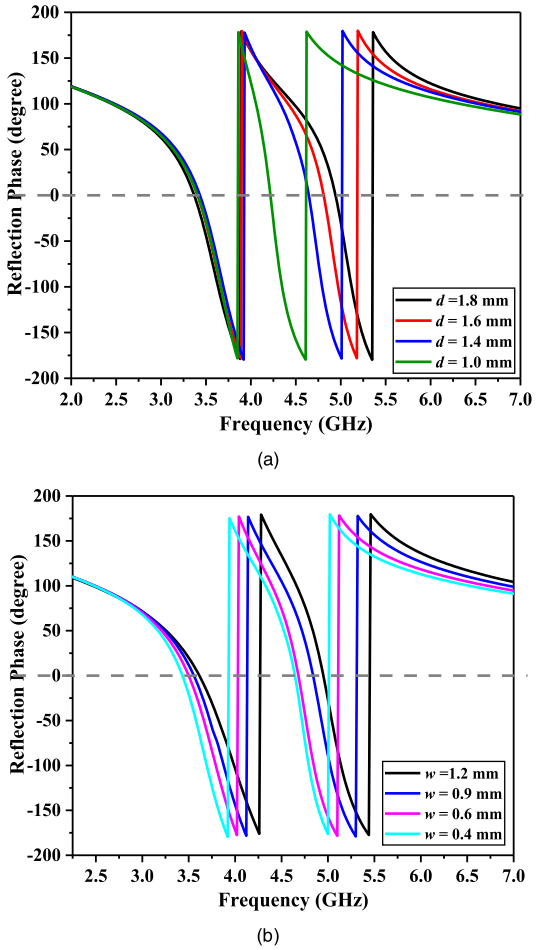

FIGURE 9. The phases of the reflection coefficients with different values of (a) d, and (b) w.

TABLE 2. Physical parameters for the proposed AMC unit cell.

Parameters	Value(mm)	Parameters	Value(mm)
w_0	18	w_1	15.9
w_2	0.2	w_3	14.8
w_4	0.4	w_5	1
w_6	0.3	w_7	10.4
w_8	0.5	R	4.12
g	0.5	r	1

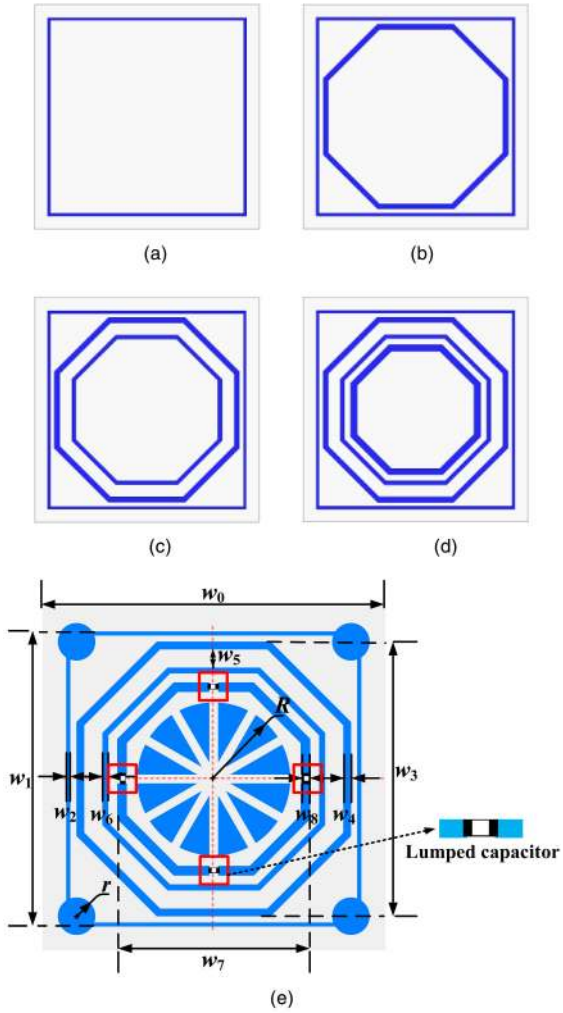

FIGURE 10. Evolution of the AMC unit cell: (a) AMC I, (b) AMC II, (c) AMC III, (d) AMC IV, and (e) AMC V.

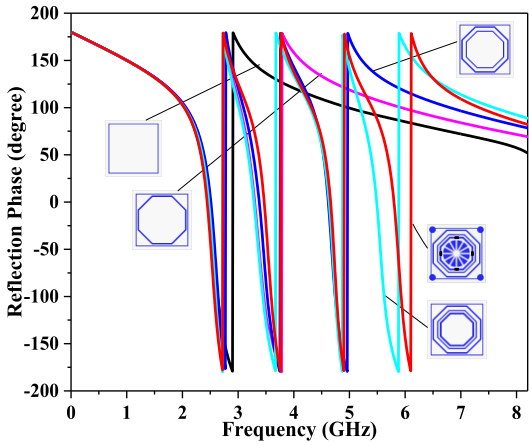

FIGURE 11. Reflection phases for the evolution of AMC unit cell.

four metallic rings, the tri-band and quad-band AMCs can be developed as shown in Fig. 11.

It is found that, by only employing the metallic four-ring structure in the AMC unit cell is difficult to generate the desired four bands exactly, especially for the highest frequency band. To realize the AMC with the zero-phases of the reflection coefficient at the aimed four frequency points, two more steps have been taken towards the four-ring AMC (AMC IV). The first step is to add four small circles at the four corners of the square ring and a central circle etched with radial slots on AMC IV. The second step is to connect four identical lumped capacitors to the innermost ring of the structure. Thus, by selecting an appropriate capacitance value ($C = 1.2$ pF), and by optimizing the physical structure, the proposed AMC (AMC V) shows the four zero-phases in

the reflection coefficient for the frequencies at 2.45, 3.5, 4.6, and 5.8 GHz as shown in Fig. 12.

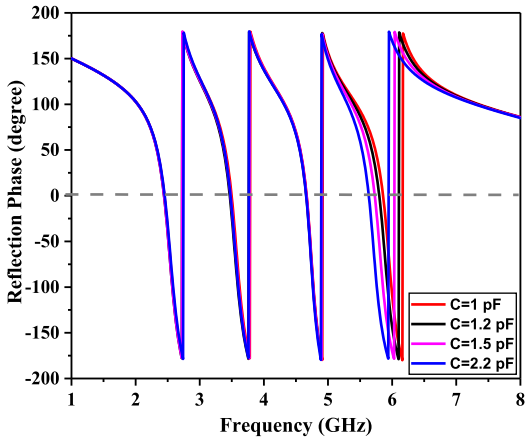

FIGURE 12. Reflection phases for different C.

The lumped capacitors used in this work are quite cheap, which is about 1$ for 1000 capacitors. Meanwhile, utilizing the lumped capacitors in the AMC structure will decrease the design cost of the AMC and improve its performance. In order to improve the AMC's performance in terms of operation frequency points, bandwidths, and miniaturization dimensions, the lumped capacitors or varactor diodes are often employed and embedded into the metal pattern of the AMC unit cells [20], [25], [32]. As illustrated in [20], there are four lumped capacitors used in one AMC unit cell. In [25] and [32], the number of varactor diodes mounted in the one AMC unit cell is eight and one, respectively. Similarly, in this research, to generate the highest frequency band, four identical lumped capacitors are embedded in the innermost ring of the proposed FMNR-AMC unit cell.

The surface current distributions for the presented quad-band AMC are displayed in Fig. 13. Obviously, the four resonant frequencies are highly correlated with the four metallic rings. At 2.45 GHz, the currents mainly flow around the utmost square ring, then extent to the inner one at 3.5 GHz. The current of the highest density concentrates along the third inner ring at 4.6 GHz, while it distributes along the innermost ring that shows the strongest current density at 5.8 GHz. Note that, these features of the surface current distributions further have validated the evolution design concept of the quad-band AMC.

C. AMC-BACKED ANTENNA

Fig. 14 shows the AMC-backed antenna system, where the multi-band antenna is placed above the center of the proposed AMC plane as an electromagnetic wave reflector with a small distance of H.

The $|S_{11}|$ for the proposed AMC-backed antenna with different values of H are displayed in Fig. 15. It is obvious that the impedance bandwidths of the AMC-backed antenna are highly sensitive to the value of H. When $H = 10$ mm,

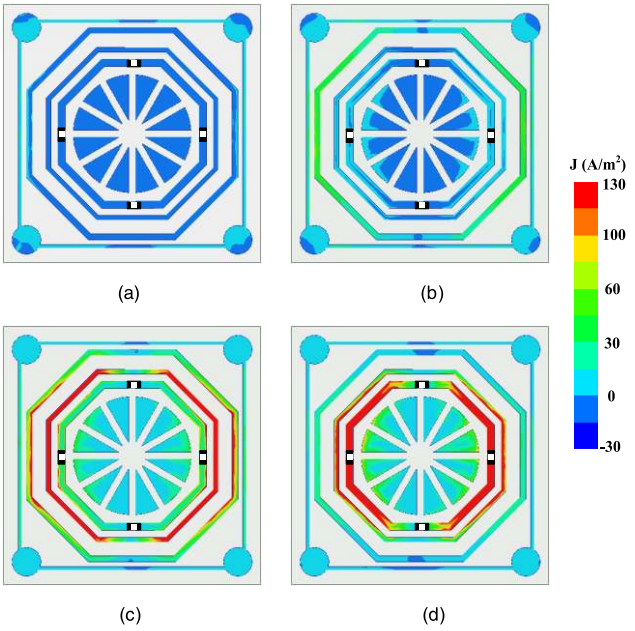

FIGURE 13. Surface current distributions of the AMC cell loaded with capacitors: (a) 2.45 GHz, (b) 3.5 GHz, (c) 4.6 GHz, and (d) 5.8 GHz.

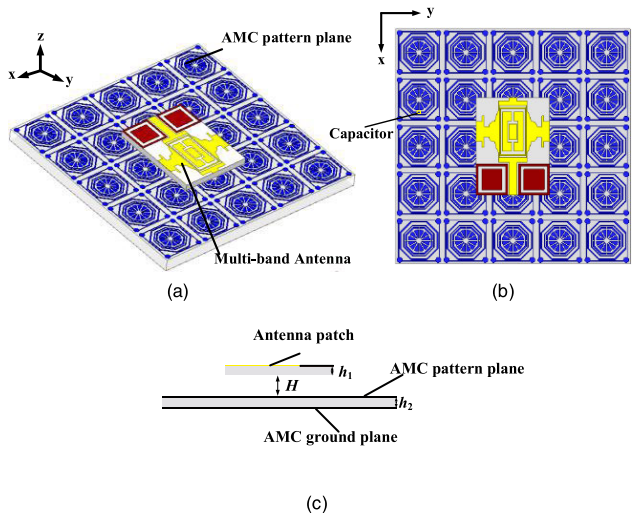

FIGURE 14. Topology of the antenna system: (a) 3D view, (b) Top view, and (c) side view. (The related parameters: $h_1 = 1.6$ mm, $h_2 = 1.6$ mm, $H = 23$ mm).

the performance of the AMC-backed antenna isn't satisfied. But if H is 23 or 30 mm, the antenna system works well with a multi-band feature. Balancing the AMC-backed antenna system's performance and its profile demand, we concluded the optimized $H = 23$ mm. Under this condition, the AMC-backed antenna's operation frequencies effectively cover three bands of 2.13 - 2.5, 3.32 - 4.81, and 5.66 - 5.87 GHz.

Fig. 16 shows the topology and reflection coefficients of the antennas with different orientation angles. In Fig. 16(a), φ represents the orientation angle which is the angle between the antenna axis and that of the AMC plane. In Fig. 16(b), it is

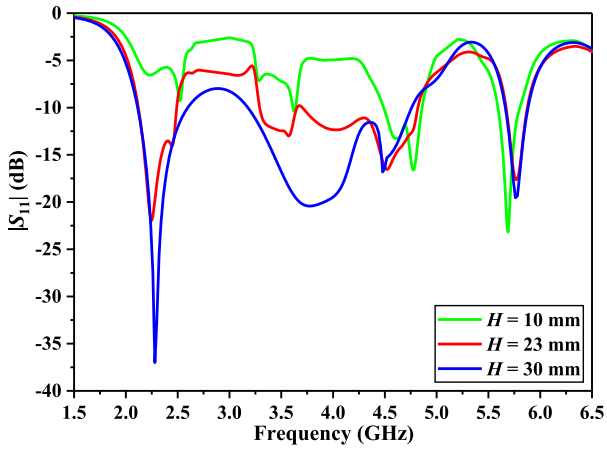

FIGURE 15. $|S_{11}|$ for the proposed AMC-backed antenna with different values of H.

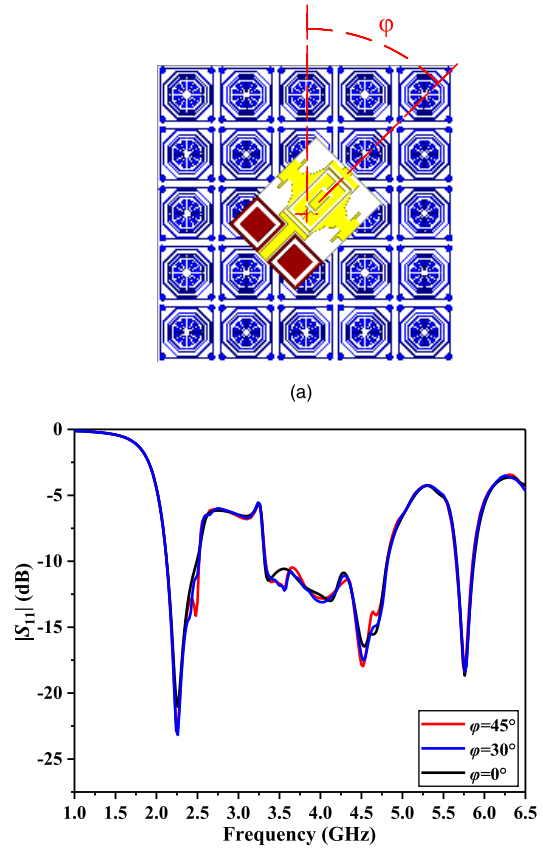

FIGURE 16. (a) Top view of the antenna system with orientation angle, φ, and (b) $|S_{11}|$ of the antennas with different values of φ.

apparent that, there are little differences among the antennas with different orientation angles of 0°, 30°, and 45°. In this research, the φ is simply selected as 0°, which is same as the works reported in [11]–[29].

To explore the influences of AMC array scales on the antenna's performance, the $|S_{11}|$ of the proposed AMC-backed antenna with the different AMC array scales is displayed in Fig. 17, and the gains of the antennas with different AMC array scales are listed in Table 3. As shown in Fig. 17, there are no big difference among the reflection coefficients of the antennas with different AMC array scales, while the gains perform clearly better as the array scales become larger (see Table 3). When the array scale gets 7 × 7 unit cells, the AMC-backed antenna's gains only increase a little at 2.45 and 4.6 GHz and even do not improve at 3.5 and 5.8 GHz in comparison to that with 5 × 5 unit cells. Balancing the reflection coefficients, gains, dimensions, and the production cost, the AMC plane with 5 × 5 unit cells is preferable in the proposed design.

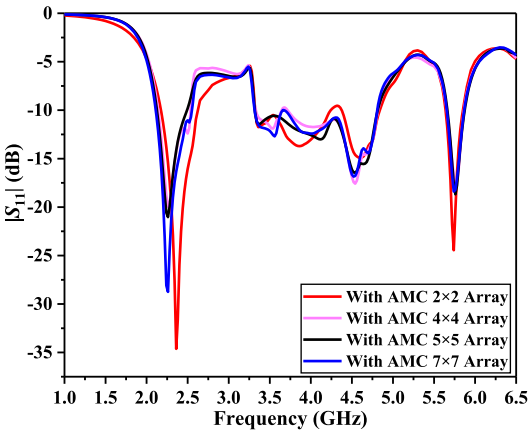

FIGURE 17. $|S_{11}|$ of the antennas with different AMC array scales.

TABLE 3. Gains of the antennas with different AMC array scales.

Scale of AMC arrays (cells × cells)	AMC-backed antenna gain (dBi)			
	2.45 GHz	3.5 GHz	4.6 GHz	5.8 GHz
2 × 2	2.1	3.4	4.1	3.8
4 × 4	5.1	6	6.3	6.3
5 × 5	5.29	7	6.4	6.7
7 × 7	5.4	7	6.7	6.7

Fig. 18 shows the current distributions of the final AMC-backed antenna at the frequencies of 2.45, 3.5, 4.6 and 5.8 GHz. As seen in these graphs, for the CPW antenna over the AMC reflector, the currents at 2.45 GHz mainly distribute around the central ellipse structure of the ornamental-pillar-shaped patch (see Fig. 18(a)), the feedline and utter side of the DGS. While at 3.5 GHz, the currents focus along the dual-slit rectangular ring. Next, at 4.6 GHz, the currents have extended to those added rectangular stubs. At 5.8 GHz (see Fig. 18(d)), current density of the CPW antenna becomes stronger as the whole DGS resonates intensively at this frequency. Along the AMC plane, there are great differences for the current distributions at the frequencies of 2.45, 3.5, 4.6 and 5.8 GHz as displayed in Fig. 18. For example, at 2.45 GHz, almost all the unit cells exist current distributions, while at 3.5 and 4.6 GHz, the currents mainly concentrate in the area of the

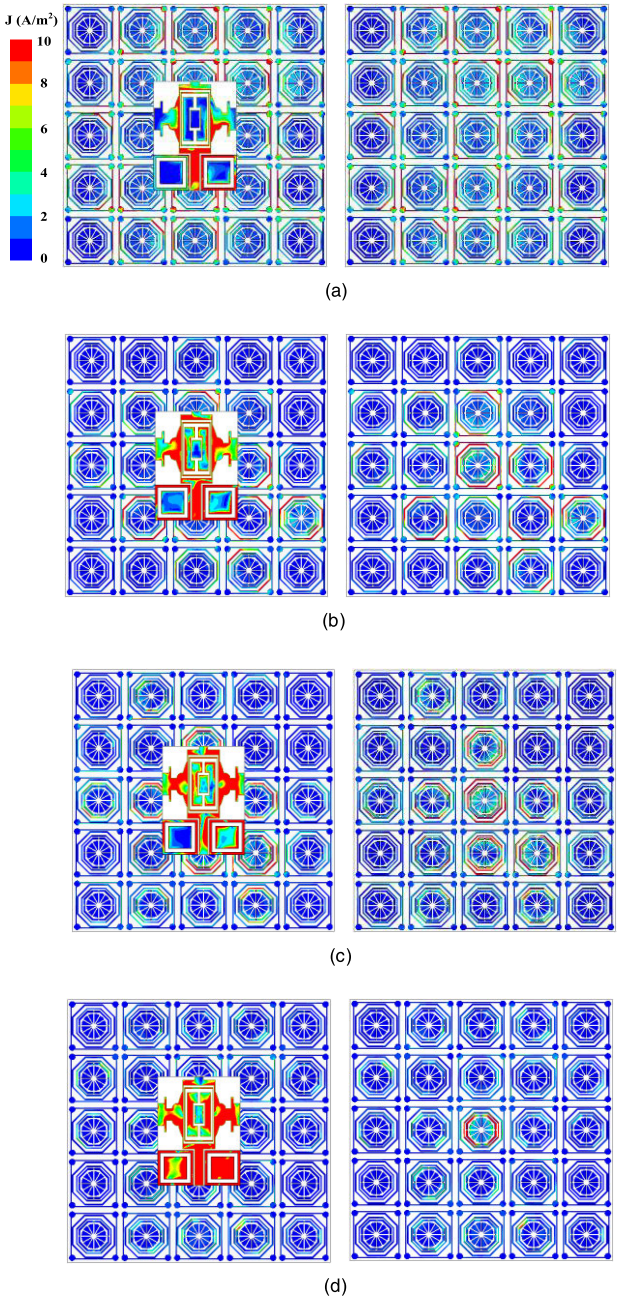

FIGURE 18. Current distributions of the AMC-backed antenna and the AMC reflector: (a) 2.45 GHz, (b) 3.5 GHz, (c) 4.6 GHz, and (d) 5.8 GHz.

central 3 × 3 array. Particularly, at 5.8 GHz, there is almost only the central single AMC cell has surface current with high density.

The 3D radiation patterns for the multi-band antenna with and without the AMC reflector are displayed in Fig. 19. It is apparent that, for the antenna only, the radiation patterns are all basically oblate and spheroidal at all the four interested frequencies, which present approximately omnidirectional radiation characteristics. While, with adding the quad-band AMC ground, the AMC-backed antenna's radiation mainly concentrates in the vertical direction above the AMC plane with high gain improvements at all the four frequencies.

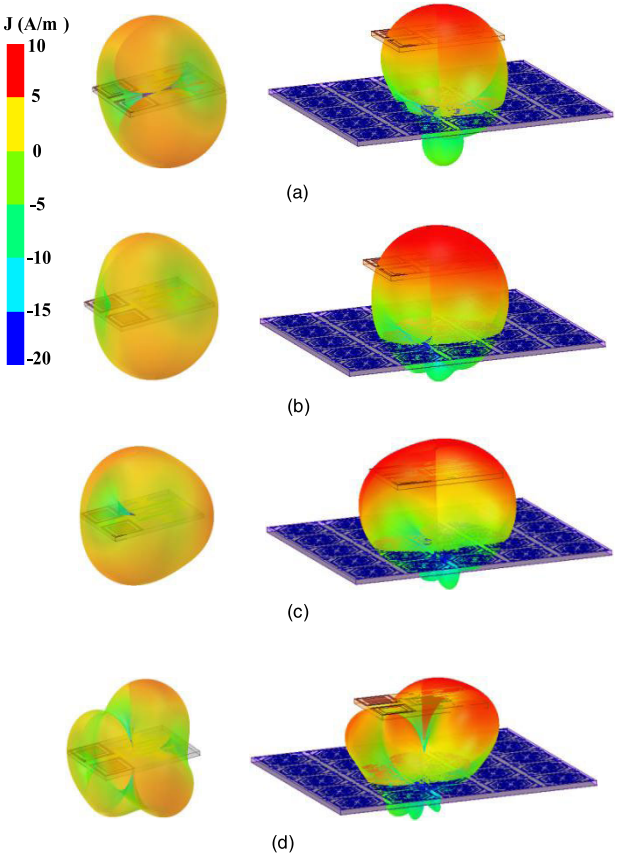

FIGURE 19. 3D radiation patterns of the antennas without and with AMC plane for (a) 2.45, (b) 3.5, (c) 4.6, and (d) 5.8 GHz.

III. MEARSUREMENT AND ANALYSIS

The proposed multi-band antenna and AMC reflector were fabricated by using a practical printed circuit board (PCB) process. Fig. 20(a) shows the prototype of the proposed antenna backed by the AMC plane with 5 × 5 unit cells and a series of lumped capacitors of 1.2 pF. The multi-band antenna is placed above the center of the AMC reflector through a 23 mm-thick foam layer. The test environment is established in a microwave anechoic chamber by using a vector network analyzer (VNA) Agilent E5071C and a standard receiving antenna as shown in Fig. 20(b).

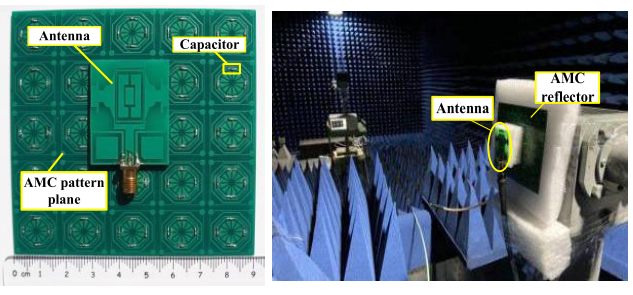

FIGURE 20. (a) Topology of antenna based on AMC reflector, (b) Microwave anechoic chamber test.

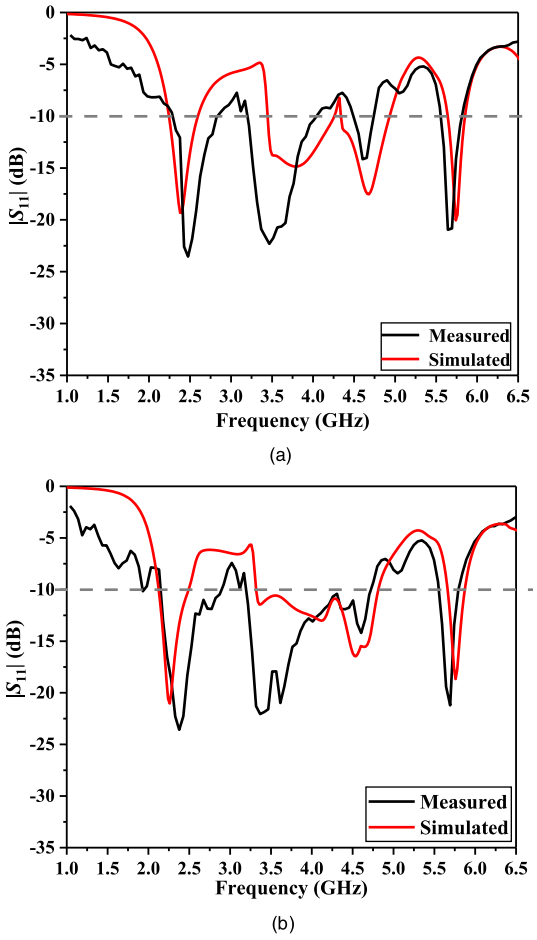

FIGURE 21. $|S_{11}|$ of antenna: (a) without AMC, (b) with AMC.

The measured $|S_{11}|$ for the multi-band antenna with and without the AMC are illustrated in Fig. 21. They are basically consistent with the simulated data. The deviation may be explained due to the fabrication tolerance, welding technique, and the test environment. It is observed in Fig. 21(a) that the antenna itself works well in all the four frequency bands, including those within 2.13–2.82, 3.22–4.01, 4.5–4.75, and 5.54–5.84 GHz, and the minimum return loss is around −20 dB at 5.8 GHz. With the quad-band AMC, the two middle frequency bands of the antenna have merged effectively into a broader one, which makes the AMC-backed antenna covers the frequency ranges of 2.13–2.87, 3.22–4.75, and 5.54–5.86 GHz, with the corresponding relative bandwidths of 14.8%, 38.4%, and 5.3%. The minimum reflection coefficient is about −23.5 dB at 2.45 GHz. It is worth noting that, the distance between the antenna and AMC plane, H, is 23 mm (0.19λ). It is much less than 30.5 mm (0.25λ), normally used for a perfect electric conductor (PEC) reflector, where λ denotes the wavelength in free space at 2.45 GHz.

Fig. 22 displays the radiation patterns of the proposed AMC-backed antenna at the frequencies of 2.45, 3.5, 4.6, and 5.8 GHz. It is apparent that, due to the impact of the AMC plane's quad-band in-phase reflecting characteristics,

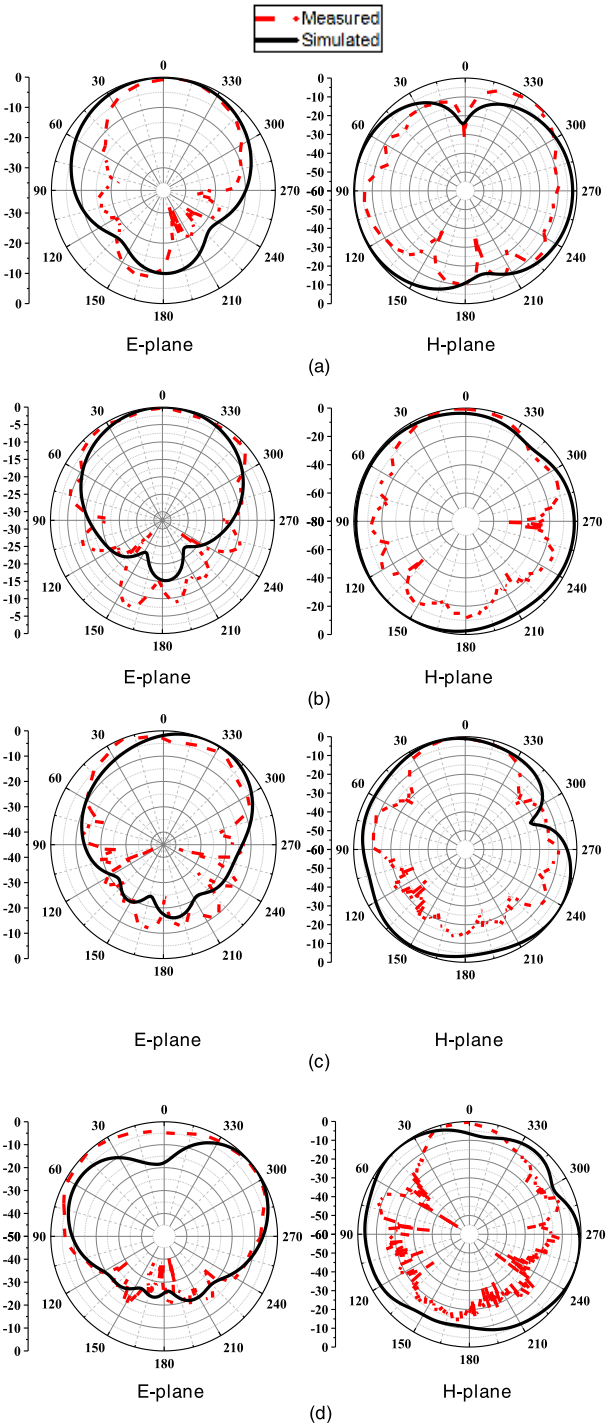

FIGURE 22. Radiation patterns of the antenna with AMC at (a) 2.45, (b) 3.5, (c) 4.6, and (d) 5.8 GHz.

the radiating energies are mainly concentrated to the upper half space in E-plane. This implies a great gain improvement realized by the AMC-backed antenna. In fact, compared with the antenna without AMC, the gains at 2.45, 3.5, 4.6, and 5.8 GHz, increase by 4.93, 5.92, 5.54 and 4.95 dB. This indicates that the gain enhancements have been achieved by about 158%, 122%, 110%, and 169%. It is also found that

TABLE 4. Comparisons among this work and previous studies.

Ref	Size of AMC-backed Ant. ($\lambda \times \lambda$)	Operation frequencies of the antenna with AMC (GHz)	Relative bandwidths of the AMC-backed antenna	Number of AMC's bands	Height of the overall antenna	Max. gain enhancement (dB)	Substrate of AMC
[12]	1.47×1.47	1.7–2.7	45.5%	1	0.25λ	N/A	FR-4
[13]	0.85×0.85	2.4–2.5	4.1%	1	0.052λ	4	RO3003
[14]	0.96×1.53	7.7–12.6	48.3%	1	0.076λ	4.1	FR-4
[15]	1.53×1.53	2.2–2.5, 5.03–5.86	16.5%	2	0.03λ	4	Textile
[16]	0.64×0.64	2.25–2.73, 4.3–6.05	19.3%, 33.8%	2	0.16λ	N/A	Cer-10
[22]	0.68×0.68	1.56–1.59, 2.43–2.45	1.9%, 0.4%	2	0.05λ	5.1/5.08	RO3003C
[23]	0.64×0.64	0.90–0.93, 2.43–2.47	3.3%, 2.1%	2	0.09λ	2.52	FR-4
[26]	0.78×0.78	3.7–4.1, 6.1–6.2, 9–9.2	10.3%, 1.6%, 2.2%	3	0.28λ	4.95	FR-4
[28]	0.72×0.72	3.33–3.39, 5.92–6.2, 9–9.2	1.8%, 4.6%, 2.2%	3	0.05λ	3.58	FR-4
[33]	0.58×0.58	1.24–1.52, 1.49–1.65	2%, 1%	2	0.03λ	N/A	F4BM-2
This work	0.73×0.73	2.13–2.87, 3.22–4.75, 5.54–5.86	14.8%, 38.4%, 5.3%	4	0.21λ	5.92	FR-4

* The λ denotes the wavelength in free space at the center frequency of single-band antenna or the center frequency of the lowest band for dual-/tri-band antenna.

in H-plane, the AMC-backed antenna exhibits a bidirectional pattern at 2.45 GHz but nearly maintain omnidirectional ones for other frequency bands.

A comparison between the proposed multi-band AMC-backed antenna and the recently published antenna systems along with AMC reflectors is summarized in Table 4. It is noticed that the presented AMC structure is characterized with the four zero-phases in the reflection coefficient. This AMC-backed antenna exhibits the maximum gain enhancement and possesses three largest relative frequency bandwidths in comparison to other tri-band AMC-backed antennas [26], [28]. Meanwhile, the size of the presented AMC-backed antenna is smaller than the works reported in [12]–[15], and [26]. Furthermore, the proposed AMC-backed antenna has relatively low profile and can be potentially applied to the applications of WLAN, WiMAX, and 5G mobile communication systems.

IV. CONCLUSION

A novel multi-band AMC-backed antenna is presented in this paper. The designed AMC unit cell consists of four metallic nested-rings (FMNR) with four lumped capacitors. It exhibits the characteristic of four zero-phases of the reflection coefficient. The measured results show that the proposed AMC-backed antenna works well in the three frequency bands of 2.13–2.87, 3.22–4.75, and 5.54–5.86 GHz with the high radiation gains. In comparison to the multi-band antenna without AMC, the AMC-backed antenna achieves a gain enhancement by the amounts of 4.93, 5.92, 5.54 and 4.95 dB at the frequencies of 2.45, 3.5, 4.6 and 5.8 GHz. In addition, the proposed AMC-backed antenna system is low profile and suitable for the applications of WLAN, WiMAX, as well as 5G mobile communication system.

REFERENCES

[1] M. Zavvari, R. Ebadzadeh, and M. Mohammadifar, "Localised surface plasmons of a corrugated metal–insulator–metal ring resonator for enhanced multiband antenna," *Electron. Lett.*, vol. 54, no. 3, pp. 120–122, Feb. 2018.

[2] T. Dabas, B. K. Kanaujia, D. Gangwar, A. K. Gautam, and K. Rambabu, "Design of multiband multipolarised single feed patch antenna," *IET Microw., Antennas Propag.*, vol. 12, no. 15, pp. 2372–2378, Dec. 2018.

[3] Y. F. Cao, S. W. Cheung, and T. I. Yuk, "A multiband slot antenna for GPS/WiMAX/WLAN systems," *IEEE Trans. Antennas Propag.*, vol. 63, no. 3, pp. 952–958, Mar. 2015.

[4] A. T. Abed, M. S. J. Singh, and M. T. Islam, "Compact fractal antenna circularly polarised radiation for Wi-Fi and WiMAX communications," *IET Microw., Antennas Propag.*, vol. 12, no. 14, pp. 2218–2224, Nov. 2018.

[5] T. Ijiguchi, D. Kanemoto, K. Yoshitomi, K. Yoshida, A. Ishikawa, S. Fukagawa, N. Kodama, A. Tahira, and H. Kanaya, "Circularly polarized one-sided directional slot antenna with reflector metal for 5.8-GHz DSRC operations," *IEEE Antennas Wireless Propag. Lett.*, vol. 13, pp. 778–781, Apr. 2014.

[6] S. E. Melais and T. M. Weller, "A quasi Yagi antenna backed by a metal reflector," *IEEE Trans. Antennas Propag.*, vol. 56, no. 12, pp. 3868–3872, Dec. 2008.

[7] A. R. Vaidya, R. K. Gupta, S. K. Mishra, and J. Mukherjee, "Right-hand/left-hand circularly polarized high-gain antennas using partially reflective surfaces," *IEEE Antennas Wireless Propag. Lett.*, vol. 13, pp. 431–434, Feb. 2014.

[8] G. Das, A. Sharma, R. K. Gangwar, and M. S. Sharawi, "Performance improvement of multiband MIMO dielectric resonator antenna system with a partially reflecting surface," *IEEE Antennas Wireless Propag. Lett.*, vol. 18, no. 10, pp. 2105–2109, Oct. 2019.

[9] A. P. Feresidis and J. C. Vardaxoglou, "High gain planar antenna using optimised partially reflective surfaces," *IEE Proc.-Microw., Antennas Propag.*, vol. 148, no. 6, pp. 345–350, Dec. 2001.

[10] J. Mu, H. Wang, H. Wang, and Y. Huang, "Low-RCS and gain enhancement design of a novel partially reflecting and absorbing surface antenna," *IEEE Antennas Wireless Propag. Lett.*, vol. 16, pp. 1903–1906, Mar. 2017.

[11] G. Li, H. Zhai, L. Li, C. Liang, R. Yu, and S. Liu, "AMC-loaded wideband base station antenna for indoor access point in MIMO system," *IEEE Trans. Antennas Propag.*, vol. 63, no. 2, pp. 525–533, Feb. 2015.

[12] J. Wu, S. Yang, Y. Chen, S. Qu, and Z. Nie, "A low profile dual-polarized wideband omnidirectional antenna based on AMC reflector," *IEEE Trans. Antennas Propag.*, vol. 65, no. 1, pp. 368–374, Jan. 2017.

[13] A. Munir, M. Aprizal, L. O. Nur, and B. S. Nugroho, "Development of bendable antenna reflector based on artificial magnetic conductor," in *Proc. Int. Symp. Antennas Propag. (ISAP)*, Busan, South Korea, Oct. 2018, pp. 1–2.

[14] H. Malekpoor and S. Jam, "Improved radiation performance of low profile printed slot antenna using wideband planar AMC surface," *IEEE Trans. Antennas Propag.*, vol. 64, no. 11, pp. 4626–4638, Nov. 2016.

[15] S. Yan, P. J. Soh, and G. A. E. Vandenbosch, "Low-profile dual-band textile antenna with artificial magnetic conductor plane," *IEEE Trans. Antennas Propag.*, vol. 62, no. 12, pp. 6487–6490, Dec. 2014.

[16] H. H. Tran and I. Park, "A dual-wideband circularly polarized antenna using an artificial magnetic conductor," *IEEE Antennas Wireless Propag. Lett.*, vol. 15, pp. 950–953, Oct. 2016.

[17] S. Shi, P. Yang, L. Zhou, and W. Chen, "Wideband planar dipole based on dual-layer artificial magnetic conductor," *J. Eng.*, vol. 2019, no. 19, pp. 6180–6183, Oct. 2019.

[18] S. Shi, P. Yang, W. Feng, L. Zhou, Q. Lu, W. Chen, and W. Che, "Wideband planar phased array antenna based on artificial magnetic conductor surface," *IEEE Trans. Circuits Syst. II, Exp. Briefs*, early access, Dec. 12, 2019, doi: 10.1109/TCSII.2019.2958984.

[19] S. M. Rouzegar, A. Alighanbari, and O. M. Ramahi, "Wideband uniplanar artificial magnetic conductors based on curved coupled microstrip line resonators," *IEEE Microw. Wireless Compon. Lett.*, vol. 27, no. 4, pp. 326–328, Apr. 2017.
[20] D. Chen, W. Yang, W. Che, Q. Xue, and L. Gu, "Polarization-reconfigurable and frequency-tunable dipole antenna using active AMC structures," *IEEE Access*, vol. 7, pp. 77792–77803, May 2019.
[21] Q. Liu, H. Liu, W. He, and S. He, "A low-profile dual-band dual-polarized antenna with an AMC reflector for 5G communications," *IEEE Access*, vol. 8, pp. 24072–24080, Jan. 2020.
[22] K. N. Paracha, S. K. A. Rahim, P. J. Soh, M. R. Kamarudin, K.-G. Tan, Y. C. Lo, and M. T. Islam, "A low profile, dual-band, dual polarized antenna for indoor/outdoor wearable application," *IEEE Access*, vol. 7, pp. 33277–33288, Feb. 2019.
[23] S. Sarkar and B. Gupta, "A dual-band circularly polarized antenna with a dual-band AMC reflector for RFID readers," *IEEE Antennas Wireless Propag. Lett.*, vol. 19, no. 5, pp. 796–800, May 2020, doi: 10.1109/LAWP.2020.2980325.
[24] H. Zhai, K. Zhang, S. Yang, and D. Feng, "A low-profile dual-band dual-polarized antenna with an AMC surface for WLAN applications," *IEEE Antennas Wireless Propag. Lett.*, vol. 16, pp. 2692–2695, Aug. 2017.
[25] T. Li, H. Yang, Q. Li, X. Zhu, X. Cao, J. Gao, and Z. Wu, "Dual-polarised and ultra-thin broadband AAMCs for both P and L bands applications," *IET Microw., Antennas Propag.*, vol. 13, no. 2, pp. 185–189, Feb. 2019.
[26] A. Ghosh, T. Mandal, and S. Das, "Design of triple band slot-patch antenna with improved gain using triple band artificial magnetic conductor," *Radioengineering*, vol. 25, no. 3, pp. 442–448, Sep. 2016.
[27] C. Yu, S. Yang, Y. Chen, and D. Zeng, "Radiation enhancement for a triband microstrip antenna using an AMC reflector characterized with three zero-phases in reflection coefficient," *J. Electromagn. Waves Appl.*, vol. 33, no. 14, pp. 1846–1859, Jul. 2019.
[28] A. Ghosh, V. Kumar, G. Sen, and S. Das, "Gain enhancement of triple-band patch antenna by using triple-band artificial magnetic conductor," *IET Microw., Antennas Propag.*, vol. 12, no. 8, pp. 1400–1406, Jul. 2018.
[29] Y. Dong, H. Toyao, and T. Itoh, "Design and characterization of miniaturized patch antennas loaded with complementary split-ring resonators," *IEEE Trans. Antennas Propag.*, vol. 60, no. 2, pp. 772–785, Feb. 2012.
[30] Y. Zheng, J. Gao, Y. Zhou, X. Cao, H. Yang, S. Li, and T. Li, "Wideband gain enhancement and RCS reduction of Fabry–Perot resonator antenna with chessboard arranged metamaterial superstrate," *IEEE Trans. Antennas Propag.*, vol. 66, no. 2, pp. 590–599, Feb. 2018.
[31] D. Mathur, S. K. Bhatnagar, and V. Sahula, "Quick estimation of rectangular patch antenna dimensions based on equivalent design concept," *IEEE Antennas Wireless Propag. Lett.*, vol. 13, pp. 1469–1472, Jul. 2014.
[32] F. Costa, A. Monorchio, S. Talarico, and F. M. Valeri, "An active high-impedance surface for low-profile tunable and steerable antennas," *IEEE Antennas Wireless Propag. Lett.*, vol. 7, pp. 676–680, Sep. 2008.
[33] J. Lin, Z. Qian, W. Cao, S. Shi, Q. Wang, and W. Zhong, "A low-profile dual-band dual-mode and dual-polarized antenna based on AMC," *IEEE Antennas Wireless Propag. Lett.*, vol. 16, pp. 2473–2476, Jul. 2017.
[34] J. H. Yoon, E. Y. Kim, Y. Lim, and Y. J. Yoon, "Equivalent circuit model and reflection phase control methods for dual-band AMC," in *Proc. 5th Eur. Conf. Antennas Propa. (EUCAP)*, Rome, Italy, Apr. 2011, pp. 1222–1226.
[35] D. Sievenpiper, L. Zhang, R. F. J. Broas, N. G. Alexopolous, and E. Yablonovitch, "High-impedance electromagnetic surfaces with a forbidden frequency band," *IEEE Trans. Microw. Theory Techn.*, vol. 47, no. 11, pp. 2059–2074, Nov. 1999.

YAJIE GONG is currently pursuing the B.S. degree with the Department of Communication Engineering, Communication University of China (CUC). Her current research interests include active AMCs and AMC-based antennas.

SHUHUI YANG (Member, IEEE) received the B.Sc. degree from Zhejiang University, in 1994, the M.Sc. degree from the Beijing Broadcasting Institute, in 1997, and the Ph.D. degree from the Institute of Microelectronics, Chinese Academy of Sciences, in 2003.

From 2003 to 2015, he was a Professor with Beijing Information and Science Technology University. He was a Visiting Scholar and an Adjunct Associate Professor with the University of South Carolina (USC), Columbia, SC, USA, in 2008. From 2013 to 2014, he was a Visiting Professor with USC. He joined the Communication University of China, as a Professor, in 2015, where he is currently the Chairman of the Department of Communication Engineering. He is a Senior Member of the Chinese Institute of Electronics (CIE). He has published more than 90 articles in technical journals and conferences and coauthored over five books. His current research interests include AMC-based antennas, MIMO antennas, filters, and metamaterials.

BIN LI received the B.Sc. and Ph.D. degrees from Northern Jiaotong University, China, in 2001 and 2007, respectively.

Since 2008, she has been a Lecturer with the Communication University of China. Her current research interests include optical fiber communication, millimeter wave devices, and terahertz components.

YINCHAO CHEN (Senior Member, IEEE) received the Ph.D. degree in electrical engineering from the University of South Carolina.

He has worked with the University of Illinois at Urbana-Champaign (UIUC), The Hong Kong Polytechnic University (HKPU), and University of South Carolina (USC). He is one of the coauthors or editors for three academic books and ten book chapters in electrical engineering. He has published more than 200 academic articles in international journals and conference proceedings. His current research interests include signal integrity for high-speed circuits, RF and integrated microwave circuits, and integrated microstrip antennas.

FANGLU TONG is currently pursuing the B.S. degree with the Department of Communication Engineering, Communication University of China (CUC). Her current research interests include AMC-based antennas and metasurfaces.

CHENYIN YU received the B.S. degree from the Communication University of China (CUC), in 2017, where she is currently pursuing the master's degree with the Department of Communication Engineering. Her current research interests include MIMO antennas and metasurfaces.